AIP | Journal of Applied Physics

Ruling out the impact of defects on the below band gap photoconductivity of Ti supersaturated Si

J. Olea, D. Pastor, A. del Prado, E. García-Hemme, R. García-Hernansanz et al.

Citation: J. Appl. Phys. **114**, 053110 (2013); doi: 10.1063/1.4817254

View online: http://dx.doi.org/10.1063/1.4817254

View Table of Contents: http://jap.aip.org/resource/1/JAPIAU/v114/i5

Published by the AIP Publishing LLC.

JOURNAL OF APPLIED PHYSICS **114**, 053110 (2013)

Ruling out the impact of defects on the below band gap photoconductivity of Ti supersaturated Si

J. Olea,[1,2] D. Pastor,[1,2,3] A. del Prado,[2,3] E. García-Hemme,[2,3] R. García-Hernansanz,[2,3] I. Mártil,[2,3] and G. González-Díaz[2,3]
[1]*Inst. de Energía Solar, E.T.S.I. de Telecomunicación, Univ. Politécnica de Madrid, 28040 Madrid, Spain*
[2]*C.E.I. Campus Moncloa, U.C.M.-U.P.M., 28040 Madrid, Spain*
[3]*Dpto. Física Aplicada III (Electricidad y Electrónica), Fac. de Ciencias Físicas, Univ. Complutense de Madrid, 28040 Madrid, Spain*

(Received 24 May 2013; accepted 16 July 2013; published online 7 August 2013)

In this study, we present a structural and optoelectronic characterization of high dose Ti implanted Si subsequently pulsed-laser melted (Ti supersaturated Si). Time-of-flight secondary ion mass spectrometry analysis reveals that the theoretical Mott limit has been surpassed after the laser process and transmission electron microscopy images show a good lattice reconstruction. Optical characterization shows strong sub-band gap absorption related to the high Ti concentration. Photoconductivity measurements show that Ti supersaturated Si presents spectral response orders of magnitude higher than unimplanted Si at energies below the band gap. We conclude that the observed below band gap photoconductivity cannot be attributed to structural defects produced by the fabrication processes and suggest that both absorption coefficient of the new material and lifetime of photoexcited carriers have been enhanced due to the presence of a high Ti concentration. This remarkable result proves that Ti supersaturated Si is a promising material for both infrared detectors and high efficiency photovoltaic devices. © *2013 AIP Publishing LLC*. [http://dx.doi.org/10.1063/1.4817254]

I. INTRODUCTION

The photovoltaic technology has been evolving faster and faster in the last years, feeding from the microelectronics knowledge.[1] The approaching of the exhausting of the non-renewable energy sources could drive it to reach higher efficiency limits. The task of obtaining low cost and high efficiency photovoltaic devices has been set out in the context of the Third Generation of Photovoltaics,[2] and new striking concepts such as the multi-junction solar cell, the intermediate band solar cell (IBSC), or the hot carriers solar cell have emerged. The IBSC approach is based on the formation of a third band, the intermediate band (IB), inside the forbidden band gap of a semiconductor.[3] This new band could be used as an intermediary to pump electrons from the valence band (VB) to the conduction band (CB) by two steps, absorbing photons of energy lower than the band gap. The addition of the photocurrent generated in this manner to the photocurrent generated by the electrons pumped from the VB directly to the CB could lead to an increase in the device efficiency. The IBSC concept aims to diminish one of the main power loss mechanisms that affect the current photovoltaic devices, which is the inability to take advantage of photons with energy lower than the band gap. Obtaining a Si based IBSC would be extremely interesting as the 90% of the photovoltaic market is covered by Si based solar cells. Moreover, practical IBSC based in Si can be used as reference to study the physical phenomena involved in the operation of the IBSCs. Furthermore, this kind of materials is also interesting in the infrared photodetectors field.[4]

One way to create such an IB is to introduce deep levels in the lattice of a semiconductor in a concentration high enough to surpass the insulator-metal transition limit, i.e., the Mott limit, which has been estimated[5] by a theoretical model to be around $6 \times 10^{19}\,cm^{-3}$ and corroborated experimentally.[6,7] If this limit is surpassed, the wavefunctions of the electrons associated to the deep impurities would overlap, forming a delocalized band inside the forbidden gap, rather than a collection of localized deep levels. The properties associated to this IB could drastically differ from the properties of the localized deep levels, and in particular, it has been pointed out that the Shockley-Read-Hall (SRH) recombination might be reduced once the IB is formed.[8]

The formation of Si supersaturated materials seems to have been accomplished by means of ion implantation followed by pulsed laser melting (PLM),[9] producing recently remarkable results.[10,11] Ion implantation permits to lodge a non-equilibrium concentration of deep impurities in a superficial layer but the lattice is severely damaged during the process. To recover the crystal quality, a thermal process is needed. However, traditional annealing processes are unable to produce a high quality supersaturated layer with an impurity concentration high enough to overcome the Mott limit. The main issue is that the solid solubility limit of deep impurities is usually very low.[12] Therefore, a technique out of thermodynamical equilibrium seems to be mandatory. In this scenario, the PLM technique has attracted much attention, since it permits to recover the crystal quality after ion implantation forming a supersaturated superficial layer and avoiding the formation of secondary phases.[13] A PLM process is able to melt and recrystallize the Si surface in very short times (10^{-8}–10^{-6} s), and this rapid solidification produces a strong solute trapping that can incorporate impurities well above the solid solubility limit and even over the Mott limit.[14]

Theoretical studies predict the formation of an IB in Si by the introduction of deep levels such as chalcogenides[15] or Ti[16] at a concentration over the Mott limit. Some of the basic principles of the IBSC concept have been demonstrated in these structures: optical absorption at energy below the band gap with high quality crystals[17,18] and the reduction of the non-radiative recombination.[19,20] Also, an intense research has been conducted to analyze the electrical transport properties of Ti supersaturated Si.[21,22] While the formation of an IB would show optical absorption below the band gap, spectral photoconductivity might be an advantageous technique,[23] adding information about the band structure of the material or about the recombination processes taking place as a function of the light wavelength.

Extrinsic photoconductivity, i.e., the photoconductivity originated from photons with energy lower than the band gap, has been extensively reported for deep levels in Si,[24] but the concentrations of deep impurities usually lie well below the IB formation limit. Specifically, extrinsic photoconductivity associated to Ti impurities at high concentration has been barely analyzed before[25,26] with no decisive conclusions about the origin of the phenomena.

In this paper, we continue the work developed in Ref. 20 on spectral photoconductivity of Ti implanted Si samples at concentrations above the Mott limit and subsequently PLM processed. The aim of this study is to go in depth about the processes involved in below band gap photoconductivity in this material by means of two approaches: first, fabricating thicker layers of Ti supersaturated Si to enhance photoconductivity, and second, study Si unimplanted PLM processed samples and Si implanted with Si and subsequently PLM processed samples to determine the origin of the below band gap photoconductivity in Ti supersaturated Si.

II. EXPERIMENTAL

High resistivity float zone (FZ) n-type Si samples $1 \times 1\,cm^2$ ($\rho \approx 200\,\Omega\,cm$), with a thickness of 300 μm, grown in the (111) direction, with a Hall mobility of $\mu \approx 1500\ cm^2/Vs$ and a carrier concentration of $n \approx 2.2 \times 10^{13}\,cm^{-3}$ at RT, were implanted with $^{48}Ti^+$ at high doses to overcome the Mott limit.[5] Similar samples were used to analyze the structural, electronic transport, and optical properties of Ti supersaturated Si.[13,18,22] Implantation processes were conducted in a VARIAN CF3000 Ion Implanter refurbished by Ion Beam Services with a tilt angle of $\sim 7°$ off the incident beam axis to minimize channeling effects. Two implantation processes were carried out on each sample to obtain a thicker layer, at energies of 35 and 150 keV, with doses of 10^{15} and $4 \times 10^{15}\,cm^{-2}$, respectively. The implantation parameters were designed to obtain a layer of about 200 nm with an almost constant profile. After implantation the samples were processed by means of the PLM technique to recover the crystal lattice and to surpass the Mott limit. PLM processes were performed at I. P. G. Photonics (New Hampshire, USA). PLM was conducted in air, with a KrF excimer laser (248 nm), with one 20 ns long pulse with an energy density of $1.8\,J/cm^2$. To analyze the effect of the PLM on the Si structure, some unimplanted samples were also processed. Also, some samples were implanted with $^{28}Si^+$ at 170 keV with a $10^{16}\,cm^{-2}$ dose and PLM processed at $1\,J/cm^2$ to obtain a damage profile similar to the Ti implantation. Finally, four Ti/Al triangular contacts were e-beam evaporated in the sample corners to characterize the samples with the van der Pauw technique. An unimplanted and unannealed Si reference sample and a Ti implanted but not PLM processed sample were also evaporated.

To analyze the Ti depth profile after implantation and PLM, samples were characterized by the time-of-flight secondary ion mass spectrometry (ToF-SIMS) technique in a TOF-SIMS IV model manufactured by ION-TOF, with a 25 keV pulsed Bi^{3+} beam at 45° incidence. A 10 keV voltage was used to extract the secondary ions generated and their time of flight from the sample to the detector was measured with a reflection mass spectrometer. An implanted non-annealed sample was used as a dose reference for calibration. Depth was calculated by optical profilometry measurement of the crater depth assuming a constant erosion rate.

The crystalline quality of the Ti implanted layers was determined by cross-sectional transmission electron microscopy (XTEM) and electron diffraction (ED) experiments at Evans Analytical Group (Sunnyvale, California) with a JEOL 2010 TEM working at 200 keV. XTEM samples were obtained using the *in situ* focused ion beam lift out method. Bright-field images were obtained and, simultaneously, ED patterns with a selected area of diffraction of about 50 nm were acquired. XTEM images of the Si implanted layers was carried out with a Titan^3 G2 working at 300 keV at the Instituto de Nanociencia de Aragón (Spain).

Transmittance and reflectance of implanted samples were measured at room temperature to obtain the absorption coefficient of the implanted layer in a Perkin Elmer Lambda 9 UV-VIS-IR spectrophotometer in the 0.55–1.2 eV range. Reflectance measurements were conducted using an integrating sphere photodetector, and a Si sample was used as a reference to evaluate the effect of the substrate. More details on the experimental setup have been published elsewhere.[18]

Finally, spectral photoresponse of samples was obtained by the characterization of the extrinsic photoconductivity at 90 K in the 0.1–1.2 eV range, obtaining measurable signal in the $E > 0.3$ eV range. The photoconductivity system configuration is the same as the one used in Ref. 20. Samples were measured in two different cryostats: a homemade liquid-nitrogen cryostat and a Janis closed-cycle He cryostat, both with a ZnSe window, using the van der Pauw set up. Measurements were performed at 90 K in order to reduce the noise compared to room temperature. Currents in the order of 1 mA or lower were used for the van der Pauw measurement to avoid self-heating effects. A vacuum pump was used to avoid moisture condensation at low temperature. A Bentham TMc300 monochromator with gratings in Czerny-Turner reflection configuration was used. The light sources were a 100 W quartz halogen lamp or a 22 W Nernst element, and they were calibrated with a Bentham pyrometric detector fitted with a KRS5 window. All the measurements are normalized to the incident power source. Special care was taken to irradiate homogenously the sample to fulfill the van der Pauw requirements. Measurements were carried out

with a SR830 DSP lock-in amplifier manufactured by Stanford Research Systems. For all of the measurements, the light from the source was mechanically chopped at 23.5 Hz.

III. RESULTS AND DISCUSSION

Fig. 1 shows the ToF-SIMS depth profiles of a Ti as-implanted sample and a sample Ti implanted and subsequently PLM processed at 1.8 J/cm^2. The theoretical Mott limit is also shown for reference. It can be seen that the implantation process produces a profile with a concentration above the Mott limit after the PLM, and therefore, the formation of an IB out of the Ti levels could be expected.[5] The profile of the as-implanted sample presents two peaks at about 32 and 124 nm below the surface, with a maximum concentration around 3.3×10^{20} cm^{-3}. The depths of these two peaks correspond to the projected range of each of the two implantations described in Sec. II. On the other hand, the PLM processed sample presents a more abrupt profile, reducing the thickness of the layer with concentration over the Mott limit to about 130 nm. This feature is typical of the PLM processes, since in the solidifying phase the impurities are pushed towards the surface by a segregation mechanism.[27] This effect is also responsible of the surface peak that reaches a maximum concentration of about 10^{21} cm^{-3} due to accumulation of Ti impurities. An abrupt profile is preferable for IB materials because the implantation tails would be below the Mott limit, producing a layer with a strong recombination, extremely detrimental for photovoltaic devices. This property makes PLM well suited to fabricate supersaturated materials. Another effect related to the PLM is the loss of impurities through the surface because of the explosive behavior of the recrystallization.[28] In our case, approximately a 42% of the Ti implanted dose is lost in the PLM. However, the main goal of the process was the obtaining of a concentration over the Mott limit, and this loss of Ti was previously considered.

To analyze the crystal quality of the samples, XTEM images showing the implanted layer after the PLM process are shown in Fig. 2. Fig. 2(a) shows a general view of the layer Ti implanted and PLM processed, Fig. 2(b) shows a magnified area close to the surface of the same layer and in Fig. 2(c) the ED diagram of the Ti implanted layer after PLM is presented. Fig. 2(d) shows the Si implanted Si layer after PLM. In Fig. 2(a) a layer of about 120 nm with some defects is observed. Although the recrystallization process is not perfect the layer has a very high degree of crystallinity, and there are no signs of the amorphization produced by the ion implantation. Moreover, the ED diagram in Fig. 2(c) is indistinguishable from an ED diagram of single-crystal Si, indicating that the crystalline quality is high enough so that the ED technique is not capable to detect the defects. In Fig. 2(b), structural defects separating different crystalline zones with a mean size equal to the layer thickness can be observed. Moreover, the different areas surrounding these defects have the same crystalline orientation. This points out that the layer is essentially single-crystal. Relating the XTEM image in Fig. 2(a) with the ToF-SIMS profile of the same sample in Fig. 1, it can be concluded that the defective layer corresponds to the high Ti concentration zone, while the crystal lattice in the depth range over 125 nm, in which the Ti concentration is lower (and thus the amorphization degree), has been perfectly recovered. We have to take into account that here a "high concentration" means a concentration over the Mott limit. The depth range over 125 nm was implanted with a lower concentration, but still several orders of magnitude higher than the solid solubility limit of Ti in Si.[12] We suggest that the defects are produced by an accumulation of impurities at the solid-liquid interface in the recrystallization process that produces an undercooling of the liquid phase making the front unstable.[29]

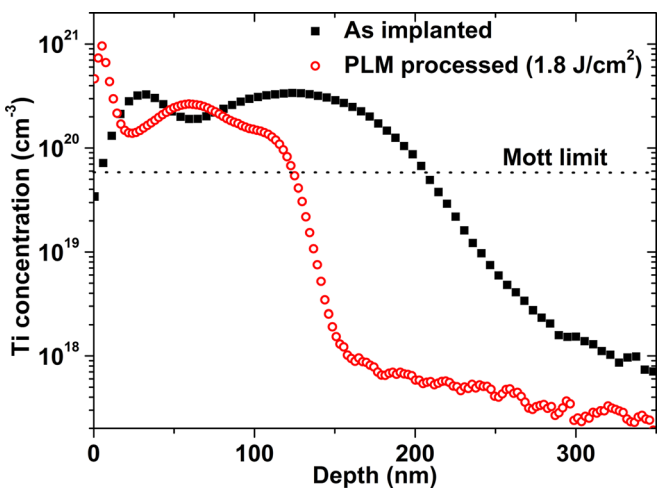

FIG. 1. Ti depth profiles obtained by the ToF-SIMS technique for a sample as-implanted and for a sample implanted and subsequently PLM processed at 1.8 J/cm^2. The theoretical Mott limit is included as a reference.

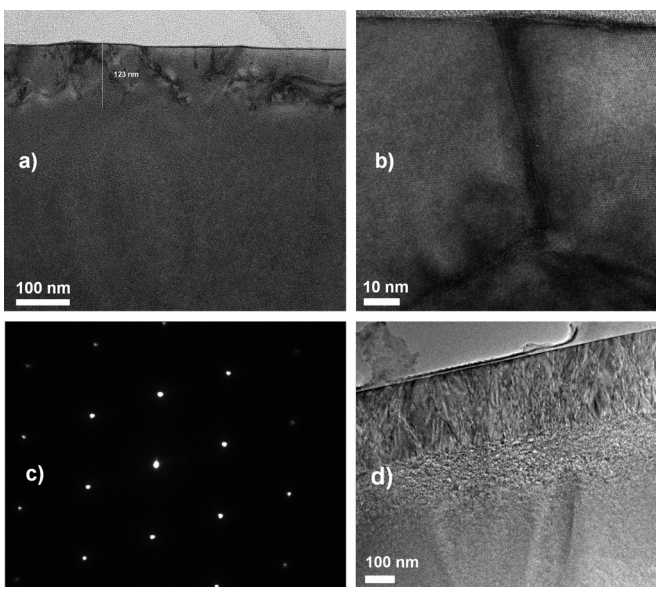

FIG. 2. (a) XTEM image of the surface of a sample Ti implanted and subsequently PLM processed at 1.8 J/cm^2 showing an area of approximately 650×650 nm^2. (b) XTEM image of the surface of a sample Ti implanted and subsequently PLM processed at 1.8 J/cm^2 showing an area of approximately 100×100 nm^2. (c) ED diagram of the layer Ti implanted and subsequently PLM processed at 1.8 J/cm^2 with a diffraction area of 50 nm. (d) XTEM image of the surface of a Si implanted Si sample PLM processed at 1 J/cm^2.

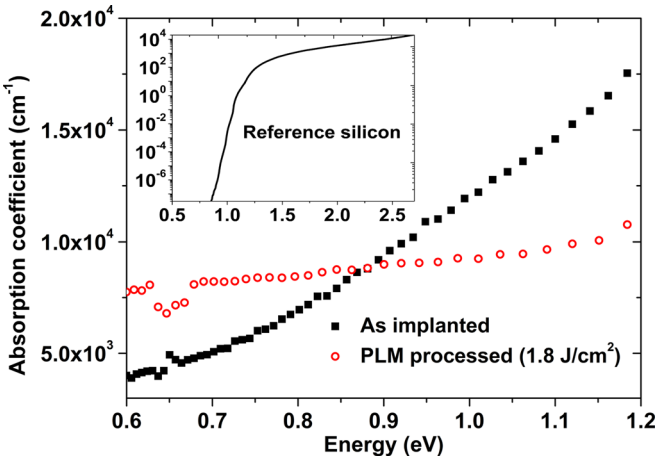

FIG. 3. Absorption coefficient as a function of the incident photon energy of a sample Ti as-implanted and of a sample Ti implanted and subsequently PLM processed at 1.8 J/cm^2. Absorption coefficient of Si has been included as a reference in the inset.

Regarding the optical properties of the implanted layers, Fig. 3 shows the absorption coefficients measured for the same samples analyzed in Fig. 1 at energies below the band gap. As it can be seen in the figure, high sub-band gap absorption coefficients have been obtained for both the Ti as-implanted and the Ti implanted and PLM processed samples. The absorption coefficient is so high that similar absorption coefficient in Si is only obtained at energies of more than 1 eV above the band gap, as it can be seen in the inset of Fig. 3.[30] The calculation of the implanted layer absorption coefficient from transmittance and reflectance measurements is confident up to 1.2 eV, since over this energy absorption in the 300 μm thick substrate predominates. The high absorption of the as-implanted sample has been attributed to the high concentration of defects produced by the implantation process. However, as the PLM processed sample has a good lattice quality, defects cannot be the source of the high absorption feature. Moreover, the absorption coefficient in the PLM processed sample is higher than the absorption coefficient of the as-implanted sample below 0.9 eV. Since the as-implanted sample is the most defective sample, the main origin of this absorption cannot be the same. Finally, the trend of the absorption coefficient is the opposite of the one expected for free carriers absorption processes. Free carriers absorption is always characterized by an increasing trend as the photon energy is decreased.[31] Therefore, the authors attributed this high absorption coefficient to the presence of a high concentration of Ti.[18]

Results for the extrinsic photoconductivity as a function of the energy of the incident photon are presented in Fig. 4. Results for a Si unimplanted reference sample, a Si sample PLM processed but not implanted, and a Si sample implanted with Si and PLM processed are shown in Fig. 4(a) while results for a sample Ti implanted but not PLM processed and a Ti implanted and PLM processed sample are shown in Fig. 4(b) along with the Si reference sample. The magnitude presented is the absolute value of the increase of the sheet conductance produced by the spectral illumination as a function of the photon energy as in Ref. 20

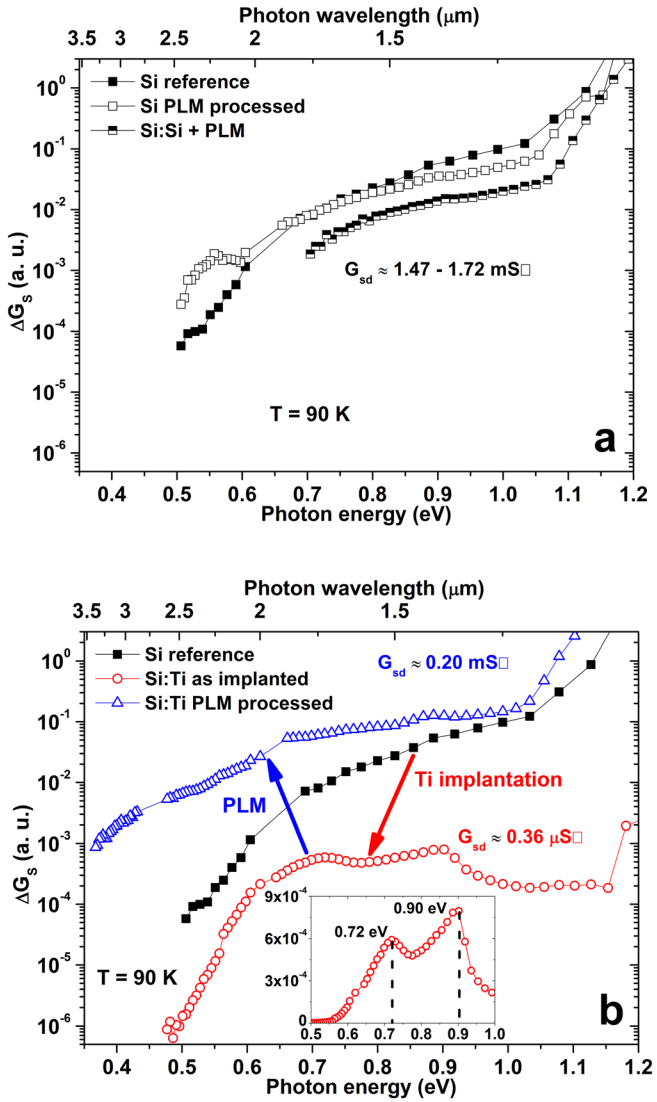

FIG. 4. Variation of the sheet conductance under illumination normalized to the incident power at 90 K as a function of the incident photon energy. (a) Si reference sample, non-implanted PLM processed Si sample and a Si sample implanted with Si and subsequently PLM processed. (b) Ti as-implanted sample and Ti implanted and subsequently PLM processed sample together with the Si reference sample. The inset shows the variation of the sheet conductance of the Ti as-implanted sample in a lineal scale.

$$\Delta G_s = \left|\frac{\Delta V}{V_d}\right| G_{sd}, \tag{1}$$

where V_d and G_{sd} are the van der Pauw voltage and sheet conductance in darkness, and ΔV is the voltage increase in the van der Pauw set up under chopped illumination. Notice that the vertical axis in both Figs. 4(a) and 4(b) is exactly the same.

Since ΔG_s is proportional to the photogenerated excess of carriers we can directly relate this magnitude to the absorption coefficient and the lifetime of carriers of the material through[32]

$$\Delta n = I_0 \alpha \eta \tau, \tag{2}$$

when $\alpha t < 1$. I_0 is the photon flux per unit of area, α is the absorption coefficient, η is the quantum yield and τ is the lifetime of carriers. We will discuss below the importance of

the substrate depending on the particular sample and also in relation to the photon energy, since the absorption coefficient of the substrate changes dramatically at energies close to the band gap.

From Fig. 4(a), we can deduce that all the samples show the intrinsic photoconductivity at energies close to the Si band gap that indicates transitions from the VB to the CB. The Si reference sample presents a decreasing ΔG_s as the energy of the incident photon is reduced. Measurable photoconductivity at energies well below the band gap for the Si reference sample would be produced by transitions involving surface states.[33,34] This feature was expected since the substrates used have high purity and therefore a high carrier lifetime that could be reducing bulk recombination. Transitions involving impurities that produce mid-gap defects are highly unlikely for the same reason. The sample PLM processed but not implanted shows a magnitude of ΔG_s almost equal to the reference. Only slight differences are found that could be attributed to differences in the wafer batch. The sample implanted with Si and PLM processed presents also a ΔG_s value close to the one of the reference sample and with the same trend. XTEM analysis of the sample Si implanted and PLM processed shown in Fig. 2(d) reveals that this sample has a poorer crystal quality than the Ti implanted sample and the defective layer is thicker. Regarding the darkness sheet conductance measurement at 90 K, all the samples of Fig. 4(a) showed almost the same value. These results would indicate that the effect of possible defects created during the PLM process or defects remaining after the post-implantation recrystallization are not important.

In Fig. 4(b), we show significative results for the Ti implanted samples. Comparing the Ti as-implanted sample to the Si reference sample, the former shows an enormous decrease of ΔG_s at all energies. The measured sheet conductance of this sample at 90 K in darkness is about 0.36 μS$\square$, i.e., almost five orders of magnitude lower than the sheet conductance of the substrate at the same temperature. This fact would mean that there is an electrical decoupling between the implanted layer and the underlying substrate. This can be concluded because in a set up as the one used in this work, if the substrate were influencing the measurement, and therefore both layers were being measured in parallel, the overall sheet conductance obtained should be higher than the sheet conductance of the substrate. The low sheet conductance measured for this sample is consistent with an amorphous layer produced due to the implantation process and the decrease in ΔG_s can be related to this amorphization. This layer would contain a high density of defects and, although the absorption coefficient in this layer is high (see Fig. 3), the defects would drastically reduce the lifetime of carriers and this would negatively affect ΔG_s. The high absorption coefficient would provide a high generation rate, but the recombination processes would dominate in this sample.

We can get deeper insight of the analyzed results of the as-implanted sample by plotting its spectrum in a lineal scale. This is shown in the inset of Fig. 4(b). ΔG_s shows two different peaks clearly resolved at about 0.72 and 0.9 eV. At energies below 0.5 eV the magnitude of ΔG_s is undetectable by our set up. The first peak could be related to an electron trap level sited at about $E_c - 0.44$ eV produced by structural defects in the Si lattice.[35,36] This correlation is fair reasonable since the implantation process would have produced a large amount of defects in the lattice. We attribute the second one to a Ti deep level that has been widely reported to be located at 0.21–0.30 eV below the CB, depending on the technique used.[37] Again, it is reasonable to find a Ti deep level as the implantation process introduced a high concentration of this impurity. These two deep levels could be the origin of the large absorption found for this sample shown in Fig. 3. Moreover, the defect levels would be acting as recombination centers decreasing the lifetime of carriers and increasing the SRH recombination.[8] As a result, this sample has a high sub-band gap absorption coefficient but a low photoconductivity.

On the other hand, the sample Ti implanted and subsequently PLM processed presents a photoconductivity that is higher than the one of the reference substrate and that is measurable in a broader range, down to about 0.35 eV. At energies close to the Si band gap the spectra of this sample increases drastically, indicating that this part of the spectrum comes mainly from optical transitions from the VB to the CB. As VB to CB transitions can be produced in both the implanted layer and in the substrate, ΔG_s values in this energy range are orders of magnitude higher than at sub-band gap energies. The increase in ΔG_s for the Ti implanted and PLM processed sample compared to the reference sample cannot be attributed to the presence of defects, since the most defective samples (Ti as-implanted sample and Si implanted and PLM processed sample) show much lower ΔG_s. This is another indication of the recovery of the crystal lattice after the PLM. In any case, the defects present in the PLM processed sample would be reducing ΔG_s with respect to a perfect crystalline supersaturated sample. Moreover, note that with the results showed in Fig. 4(a) we have previously discarded all the fabrication processes (implantation and PLM) as the origin of a photoconductivity enhancement.

As the photon energy is reduced below the band gap, the absorption coefficient and consequently the product αt in the substrate decreases drastically (see inset in Fig. 3). As ΔG_s in the sample Ti implanted and PLM processed is higher than the one of the substrate, we can conclude that below the Si band gap, the carrier generation comes mainly from the supersaturated layer. Likewise, the absorption coefficient of the implanted and PLM processed sample (see Fig. 3) is high and with a smooth variation in a broader range, similarly to the photoconductivity spectrum. It has been reported that the absorption coefficient might keep this behavior even below 0.6 eV.[18] As the Ti as-implanted sample and the Ti implanted and PLM processed sample present very similar values for the absorption coefficient, this result would indicate that the recombination processes would be reduced in the PLM processed sample in comparison with the as-implanted case. This conclusion is supported by the high crystal quality obtained for the PLM processed sample shown in Fig. 2. We suggest that once the Mott limit is surpassed, the reduction of the non-radiative recombination processes would result in a recovery of the lifetime of carriers, as it has been recently reported in Ref. 20. This

conclusion, together with the high absorption coefficient measured for this material, is a very important result for photovoltaic applications.[3,5]

In the ΔG_s spectra in Fig. 4(b) for the Ti implanted and PLM processed sample there is no sign of the peak at 0.72 eV quoted for the as-implanted sample (it is not noticeable even in lineal scale). The extinction of the defect related peak should be probably due to the recovery of the crystal lattice after the PLM. However, it is interesting to note that the Ti peak located at about 0.9 eV is still clearly resolved in a lineal scale (not shown), superimposed to the broad photoconductivity band. This is consistent with the attribution of this peak to transitions involving Ti levels.

Finally, we conclude that the appearance of an intense below band gap photoconductivity for the sample Ti implanted and PLM processed can be attributed to the high concentration of Ti. The formation of a Si supersaturated layer with a Ti concentration over the Mott limit would reduce the SRH recombination and enhance the lifetime of carriers in comparison to the localized deep levels scenario.[8] This is a striking result since the classic theory of recombination would have predicted a strong reduction of the photo-generation due to the high Ti concentration.[38] Adding this to the recrystallization of the damaged layer, and to the high absorption coefficient shown in Fig. 3, this sample has higher ΔG_s than the Si reference substrate. These conclusions are supported by the electronic transport properties measurements performed on similar samples that point to the formation of an IB in Ti supersaturated Si.[21,22] This result is of extremely importance since it demonstrates that the fabrication of Si supersaturated materials by the introduction of deep levels at a concentration over the Mott limit is feasible and that these kind of materials can be interesting for photovoltaic and optoelectronic applications.

IV. CONCLUSIONS

Ti supersaturated Si samples have been analyzed. ToF-SIMS depth profiles indicate that the theoretical Mott limit has been surpassed after the PLM, and XTEM and ED characterization point out to a good lattice reconstruction. Transmission and reflection measurements resulted in an extremely high absorption coefficient at energies below the Si band gap and the origin of this intense absorption seems to be the high concentration of Ti impurities, ruling out the possibility of having an important absorption by the defects formed during the ion implantation or the subsequent PLM process.

Photoconductivity measurements show that Ti supersaturated Si samples present a strong spectral response at energies below the band gap. This response is measurable at energies over 0.35 eV. We discarded the fabrication processes as the cause of this extremely high photoconductivity and concluded that the origin would be the extremely high Ti concentration. Results indicate that the lifetime of carriers might have been enhanced by the introduction of a Ti concentration over the Mott limit in a high quality silicon lattice. All these conclusions show the enormous potential of this material for photovoltaic and photodetectors devices.

ACKNOWLEDGMENTS

The authors would like to acknowledge the C.A.I. de Técnicas Físicas for ion implantation experiments and e-beam evaporations, the Nanotechnology and Surface Analysis Services of the Universidad de Vigo C.A.C.T.I. for ToF-SIMS measurements, Dr. J. Herrero (CIEMAT) for UV-VIS-IR measurements facilities, and the Instituto de Nanociencia de Aragón for the TEM images. J. Olea and D. Pastor thanks Professor A. Martí and Professor A. Luque for useful discussions and guidance and acknowledge financial support from the MICINN within the program Juan de la Cierva (JCI-2011-10402 and JCI-2011-11471), under which this research was undertaken. Research by E. García-Hemme has been partly supported by a PICATA predoctoral fellowship of the Moncloa Campus of International Excellence (UCM-UPM). This work was partially supported by the projects NUMANCIA II (S-2009/ENE-1477) founded by the Regional Government of Comunidad de Madrid and grant GR35/10-A founded by the Universidad Complutense de Madrid.

[1]A. Martí and A. Luque, *Next Generation Photovoltaics: High Efficiency Through Full Spectrum Utilization* (IOP Publishing, Ltd., Bristol, 2004).
[2]G. Conibeer, Mater. Today **10**, 42 (2007).
[3]A. Luque and A. Martí, Phys. Rev. Lett. **78**, 5014 (1997).
[4]M. Casalino, Int. J. Opt. Appl. **2**, 1 (2012).
[5]A. Luque, A. Martí, E. Antolín, and C. Tablero, Physica B **382**, 320 (2006).
[6]M. T. Winkler, D. Recht, M.-J. Sher, A. J. Said, E. Mazur, and M. J. Aziz, Phys. Rev. Lett. **106**, 178701 (2011).
[7]D. Pastor, J. Olea, A. del Prado, E. García-Hemme, R. García-Hernansanz, and G. González-Díaz, Sol. Energy Mater. Sol. Cells **104**, 159 (2012).
[8]A. Luque and A. Martí, Adv. Mater. **22**, 160 (2010).
[9]C. W. White, J. Narayan, and R. T. Young, Science **204**, 461 (1979).
[10]M. Tabbal, T. Kim, J. M. Warrender, M. J. Aziz, B. L. Cardozo, and R. S. Goldman, J. Vac. Sci. Technol. B **25**, 1847 (2007).
[11]G. González-Díaz, J. Olea, I. Mártil, D. Pastor, A. Martí, E. Antolín, and A. Luque, Sol. Energy Mater. Sol. Cells **93**, 1668 (2009).
[12]S. Hocine and D. Mathiot, Appl. Phys. Lett. **53**, 1269 (1988).
[13]J. Olea, M. Toledano-Luque, D. Pastor, E. San-Andrés, I. Mártil, and G. González-Díaz, J. Appl. Phys. **107**, 103524 (2010).
[14]J. Narayan, C. W. White, M. J. Aziz, B. Stritzker, and A. Walthius, J. Appl. Phys. **57**, 564 (1985).
[15]K. Sánchez, I. Aguilera, P. Palacios, and P. Wahnón, Phys. Rev. B **82**, 165201 (2010).
[16]K. Sánchez, I. Aguilera, P. Palacios, and P. Wahnón, Phys. Rev. B **79**, 165203 (2009).
[17]T. G. Kim, J. M. Warrender, and M. J. Aziz, Appl. Phys. Lett. **88**, 241902 (2006).
[18]J. Olea, A. del Prado, D. Pastor, I. Mártil, and G. González-Díaz, J. Appl. Phys. **109**, 113541 (2011).
[19]E. Antolín, A. Martí, J. Olea, D. Pastor, G. González-Díaz, I. Mártil, and A. Luque, Appl. Phys. Lett. **94**, 042115 (2009).
[20]E. García-Hemme, R. García-Hernansanz, J. Olea, D. Pastor, A. del Prado, I. Mártil, and G. González-Díaz, Appl. Phys. Lett. **101**, 192101 (2012).
[21]J. Olea, G. González-Díaz, D. Pastor, and I. Mártil, J. Phys. D: Appl. Phys. **42**, 085110 (2009).
[22]J. Olea, G. González-Díaz, D. Pastor, I. Mártil, A. Martí, E. Antolín, and A. Luque, J. Appl. Phys. **109**, 063718 (2011).
[23]A. Rose, *Concepts in Photoconductivity and Allied Problems* (Robert E. Krieger Publishing Co., New York, 1978).
[24]A. G. Milnes, *Deep Impurities in Semiconductors* (John Wiley & Sons, Inc., New York, 1973).
[25]N. T. Bagraev, L. S. Vlasenko, A. A. Lebedev, I. A. Markulov, and P. Yusupov, Phys. Status Solidi B **103**, K51 (1981).
[26]A. A. Aivazov, A. L. Giorgadze, A. E. Zemko, V. K. Prokof'eva, A. R. Salmanov, and F. R. Kashimov, Inorg. Mater. **24**, 5 (1988).

[27]C. W. White, S. R. Wilson, B. R. Appleton, and F. W. Young, Jr., J. Appl. Phys. **51**, 738 (1980).
[28]M. O. Thompson, J. W. Mayer, A. G. Cullis, H. C. Webber, N. G. Chew, J. M. Poate, and D. C. Jacobson, Phys. Rev. Lett. **50**, 896 (1983).
[29]J. Olea, D. Pastor, M. Toledano-Luque, I. Mártil, and G. González-Díaz, J. Appl. Phys. **110**, 064501 (2011).
[30]M. J. Keevers and M. A. Green, Sol. Energy Mater. Sol. Cells **41**/**42**, 195 (1996).
[31]R. H. Bube, *Electronic Properties of Crystalline Solids* (Academic, New York, 1974).
[32]N. V. Joshi, *Photoconductivity: Art, Science and Technology* (Marcel Dekker, Inc., New York, 1990). p. 17.
[33]M. Casalino, G. Coppola, M. Iodice, I. Rendina, and L. Sirleto, Sensors **10**, 10571 (2010).
[34]C. Coletti, G. Bussetti, F. Arciprete, P. Chiaradia, and G. Chiarotti, Phys. Rev. B **66**, 153307 (2002).
[35]E. Fretwurst, V. Eremin, H. Feick, J. Gerhardt, Z. Li, and G. Lindström, Nucl. Instrum. Methods Phys. Res. A **388**, 356 (1997).
[36]M. Willander, J. Appl. Phys. **56**, 3006 (1984).
[37]T. Roth, M. Rüdiger, W. Warta, and S. W. Glunz, J. Appl. Phys. **104**, 074510 (2008); L. Tilly, H. G. Grimmeiss, H. Pettersson, K. Schmalz, K. Tittelbach, and H. Kerkow, Phys. Rev. B **43**, 9171 (1991); J. R. Morante, J. E. Carceller, P. Cartujo, and J. Barbolla, Solid-State Electron. **26**, 1 (1983); M. Schulz, Appl. Phys. **4**, 225 (1974).
[38]J. R. Davis, Jr., A. Rohatgi, R. H. Hopkins, P. D. Blais, P. R. Choudhury, J. R. McCormick, and H. C. Mollenkopf, IEEE Trans. Electron Devices **27**, 677 (1980).